Surface Charge Accumulation Characteristics on DC GIL Three-post Insulators Considering the Influence of Temperature Gradient

Qi Hu, Qingmin Li, *Member*, *IEEE*, *CSEE*, Zhipeng Liu, Naifan Xue, Jian Wang, *Member*, *IEEE*, *Member*, *CSEE*, and Manu Haddad, *Member*, *IEEE*

***Abstract*—Surface charge accumulation is considered to be a critical factor in flashover failure of three-post insulators. However, surface charge accumulation characteristics on three-post insulators with complex structures and uneven electric fields are still unclear. Furthermore, the temperature gradient field makes charge accumulation more complicated. In this presentation, surface charge profiles of DC three-post insulators under electro-thermal coupling stress are studied by establishing a multi-degree-of-freedom movement measurement system. The abdominal area of the three-post insulator accumulaftes charges of identical polarity as the DC voltage, while the leg area accumulates heteropolar charges. Charge density from the bottom of the leg to the center of the abdomen presents a trimodal distribution pattern, including two homopolar charge peaks and one heteropolar charge peak. Asymmetrical surface conductance distribution arising from the temperature gradient leads to a significant increase in amplitude and distribution range of the homopolar charge peak at the legs of insulator. Increase of the temperature gradient will further magnify the homopolar charge peak at the legs. When DC voltage is 100 kV and conductive pole temperature is 70°C, surface charge density of the three-post insulator can reach 100 $\mu C/m^2$. Therefore, surface conductance regulation of the leg region is the key to charge regulation and insulation optimization design of DC three-post insulators.**

***Index Terms*—Charge accumulation, charge measurement, surface charge, temperature gradient, three-post insulator.**

I. Introduction

DIRECT current gas-insulated transmission line (DC GIL) is well known for its high transmission capacity, low energy loss and small footprint, which has broad application prospects in long-distance transmission and offshore wind power transmission [1]–[3]. Three-post insulators are responsible for supporting conductors and electrical insulation in GIL and have the advantages of providing thermal expansion and mechanical strain compensation, which is one of the indispensable key components of the GIL basic unit. However, free charges move directionally under DC voltage, which is likely to cause charge accumulation on the insulator interface, resulting in surface electric field distortion, causing surface flashover and significantly reducing insulation performance of GIL [4]–[6]. Therefore, exploring charge accumulation characteristics and dominant influencing factors of three-post insulators is crucial to insulation design and engineering application of DC GIL.

For decades, researchers have successively conducted experimental studies over the surface charge accumulation mechanism on insulators [7]–[9]. Early researchers took cylindrical or conical insulators with simplified structures as research objects and put forward many physical models for the surface charge accumulation process. However, surface charge accumulation process of insulators is vulnerable to insulator shape, temperature, metal particles, humidity, electrode roughness [10], [11]. Researchers have not reached a consensus on the mechanism of charge accumulation, and measurement results for simplified insulators can't be directly used to guide insulation design of DC GIL. Therefore, Nakanishi *et al*. design a more complex mechanical device to test surface charge density of actual basin insulators [12]. Zhang *et al*. optimize accuracy of measuring devices and processing algorithms for basin insulators, and find the surface charges of insulators in air and SF_6 gas have opposite polarities, and believe that partial discharge in the gas contributed to accumulating surface charge [13]. However, the above-mentioned experimental studies do not take the effect of temperature on charge accumulation process into consideration. A temperature gradient field is formed when GIL is carrying current normally, resulting in inconsistent distribution of electrical conductance, which highly affects charge accumulation process. Ma *et al*. design a surface potential measurement test platform for a basin-type insulator that takes into account the influence of temperature. Experimental results show that temperature gradient significantly increases surface charge density, and it is believed bulk current is the key factor in the process of accumulating charge under the temperature gradient [14], [15].

At present, surface charge profile characteristics of DC basin insulators are relatively clear, but research on accumulated surface charges of three-post insulators is rarely reported. The

Manuscript received December 21, 2021; revised March 23, 2022; accepted April 19, 2022. Date of online publication March 3, 2023; date of current version July 11, 2023. This work was supported by the National Natural Science Foundation of China (51737005, 52127812, 51929701).

Q. Hu was with North China Electric Power University, Beijing 102206, China. He is now with State Grid Jiangxi Electric Power Co., Ltd., Nanchang 330077, China.

Q. M. Li (correspoding author, email: lqmeee@ncepu.edu.cn), Z. P. Liu, N. F. Xue, and J. Wang are with the State Key Laboratory of Alternate Electrical Power System with Renewable Energy Sources, North China Electric Power University, Beijing 102206, China.

M. Haddad is with the Advanced HV Engineering Research Centre, Cardiff University, The Parade, Cardiff CF24 3AA, U.K.

DOI: 10.17775/CSEEJPES.2021.09240

reason is the structure of three-post insulators is complex, with many curved surfaces and corners, so measurement of surface charge requires more complex measurement devices and processing algorithms. However, what is noteworthy is that the electric field profile of a three-post insulator is more uneven than of the basin insulator, with the normal field concentrated on the abdomen and tangential field concentrated on the legs, whicfh leads to intensified charge accumulation in local areas [16]. In addition, insulator shape also affects the heat transfer process. Temperature distribution of three-post insulators is quite different from that of basin insulators, and impact of the temperature gradient field of a three-post insulator on the charge accumulation process is still inconclusive [17]. Current research on interface charge of basin insulators is inapplicable to guide optimal design of DC tri-post insulators.

To solve the above problems, a multi-degree-of-freedom mobile measurement system considering the effect of temperature for surface charge on three-post insulators is established, which can realize Omni-directional surface charge measurement of three-post insulators. Based on the established measurement system, the charge accumulation process on DC three-post insulators under electro-thermal coupling stress is explored, and charge accumulation characteristics and key influencing factors of three-post insulators are obtained, which lay a foundation for the optimization design of DC GIL three-post insulators.

II. Experimental Setup

A. Multi-Degree-of-Freedom Mobile Measurement System for Surface Potential

The surface potential measurement system shown in Fig. 1 is established for the complex curved surface structure of the three-post insulator. The system consists of a DC power generator, experimental chamber, surface potential measuring device, multi-axis mechanical control device, and oil bath circulating heating device. The DC power generator is concatenated to the bushing of the experimental chamber through a protection resistance and can apply a maximum DC voltage of ±300 kV to the test samples. The experimental chamber can be filled with different types of experimental gas, with the highest-pressure tolerance up to 0.8 Mpa. The surface potential measuring device consists of an electrometer (Trek 341B) and the supporting Kelvin probe (Trek 3455ET), which can measure the single-point surface potential value of the insulator and output it to the computer with a range of ±20 kV and the error less than ±0.1% of the full range. The multi-axis mechanical control device is composed of a multi-axis mechanical controller, a five-axis mechanical arm, and other components, which can control the probe to accurately scan the surface profile of the three-post insulator to obtain its overall potential distribution. The oil bath circulating heating device is composed of a modified high-voltage conductive pole, an oil storage tank, and a high-temperature oil pump. The temperature of the conductive pole is increased by the heat exchange between the high-temperature oil and the conductive pole. The temperature control range is from ambient temperature to 120°C, and the adjustment accuracy is 0.5°C.

B. Test Sample and Measurement Procedure

Test samples are made of Al_2O_3-filled epoxy resin commonly used in GIL, using the same manufacturing process as industrial. Sample shape and the electrode arrangement conform to the working state of an actual three-post insulator, as shown in Fig. 2. A three-post insulator includes an embedded tube, epoxy resin, and inserts, with 200 mm outer diameter and 60 mm inner diameter. A high-voltage conductive pole passes through the insulator, and a heated oil pump is arranged inside, which can apply electrical-thermal coupling stress to the three-post insulator. The insulator insert is connected to a removable metal enclosure to maintain good grounding. In addition, a

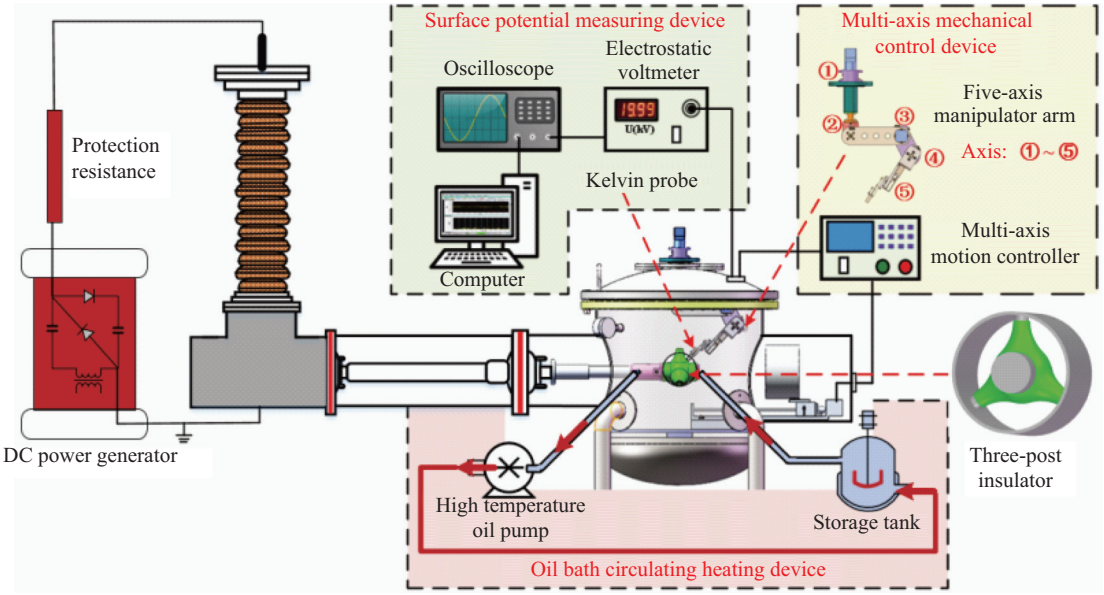

Fig. 1. Schematic diagram of surface potential measurement system for three-post insulators.

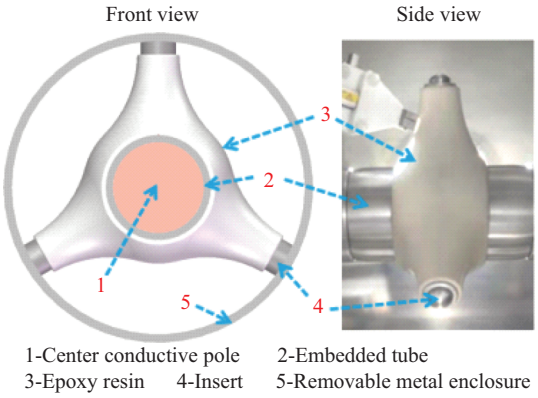

Fig. 2. Test three-post insulator and electrode arrangement.

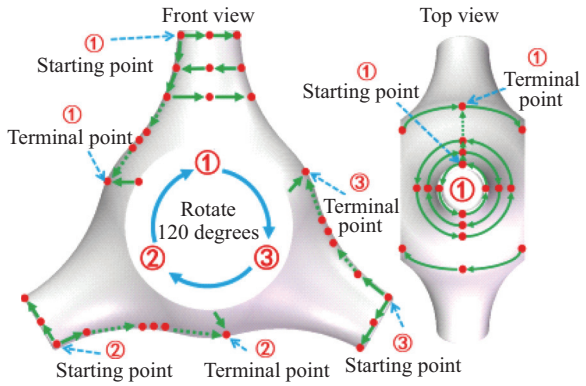

Fig. 3. Schematic diagram of Kelvin probe scanning.

shield structure is designed at the end of the conductive pole to avoid effect on the electric field.

Before each experiment, insulators are carefully cleaned with ethanol and dried at 80°C for 24 hours to minimize influence of humidity on surface conductivity. The three-post insulator is installed between coaxial cylindrical electrodes. To simplify experimental process and save experimental materials, the test platform is evacuated and filled with SF_6 gas to 0.1 MPa. After confirming experimental chamber sealing performance is good, the oil bath circulating heating device is launched to carry out temperature loading on the center conductive pole. After heating for 3 hours, DC voltage is put on the insulator and maintained for a target duration. A DC power generator is switched off during measurement and the removable metal enclosure moves away from insulator by a motorized translation stage. Subsequently, the Kelvin probe moves from its parking position, which is just outside the enclosure, to the insulator under control of the five-axis mechanical arm and scans the surface of an insulator post in a circle from top to bottom. Then, angle of the three-post insulator is adjusted by a rotating motor on a high-voltage conductive pole to test the surface of the remaining two posts. Scanning path is shown in Fig. 3. The Kelvin probe keeps perpendicular to the measured surface and maintains 3 mm throughout the measurement process. Movement error of the measuring device is less than 0.1 mm, and accumulated movement error is less than 1 mm during measurement. The measuring device automatically returns to mechanical zero point after each measurement. The number of sampling points is 5040 and test period is approximately 27 minutes.

C. Surface Charge Inversion Calculation Method

Potential measured by the Kelvin probe depends on accumulated charges at all measuring points on the insulator. Therefore, it is necessary to inversely calculate potentials of all measuring points to acquire a surface charge profile of the insulators. Therefore, a charge density matrix $\boldsymbol{Q}$ could be given by (1).

$$\boldsymbol{Q} = \boldsymbol{H}^{-1}\boldsymbol{U} \tag{1}$$

where $\boldsymbol{U}$ is measured potential, $\boldsymbol{H}$ is transfer function matrix, which can be acquired by a basic calculation formula of the electromagnetic field [18]. Dimension of the matrix is the same as number of potential sampling points.

However, it is inevitable to be interfered by noise during measurement process, which may influence accuracy and stability of the inverse calculation, especially when matrix size is so large. To solve this, Tikhonov regularization method was used to replace $\boldsymbol{H}$ matrix [19]. Estimated $\boldsymbol{Q}$ could be given by (2).

$$\boldsymbol{Q} = \left(\boldsymbol{H}^{\mathrm{T}}\boldsymbol{H} + \frac{\sigma_{\mathrm{n}}^2}{\sigma_{\mathrm{s}}^2}\boldsymbol{I}\right)^{-1}\boldsymbol{H}^{\mathrm{T}}\boldsymbol{U} \tag{2}$$

where $\boldsymbol{I}$ is a unit matrix, σ_{n}^2 and σ_{s}^2 are variances of noise and signal. Regularization parameter γ is the ratio of σ_{n}^2 to σ_{s}^2. γ is empirically selected to be 0.3% of maximum eigenvalue of matrix $\boldsymbol{H}^{\mathrm{T}}\boldsymbol{H}$ [20].

A set of verification experiments based on the dust figure were designed to verify accuracy of surface charge inversion algorithm. After putting +100 kV DC voltage on test sample for 12 hours, surface charge density is tested by the measurement and calculation method described above, and the result is shown in Fig. 4(a). Then, negatively charged red carbon dust (Huiwei CB543A) is evenly sprinkled on test sample, and the dust figure that intuitively reflects charge distribution can be acquired by utilizing characteristics of surface charge absorbing dust with heteropolar charge, as shown in Fig. 4(b). Since carbon dust is negatively charged, the area where red carbon dust is absorbed represents the area where positive charge is concentrated, and blank area represents the area where negative charge is concentrated.

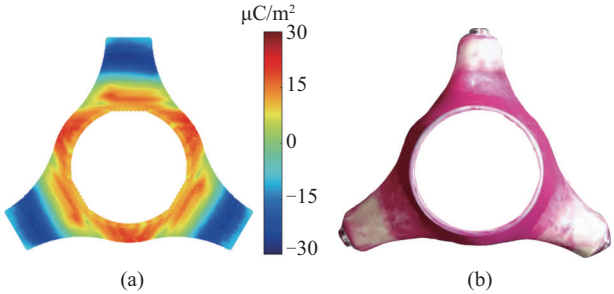

Fig. 4. Verification experiment results of surface charge. (a) Surface charge profile. (b) Dust figure.

Taking Fig. 4(a) and Fig. 4(b) into comparison, surface charge figured by the inversion algorithm is in keeping with charge distribution shown in the dust figure, which verifies availability of the measurement and calculation method for surface charge of three-post insulators.

III. Experimental Results

A. Surface Charge Profiles of DC Three-post Insulator

Figure 5 illustrates surface charge profiles of three-post insulator under ambient temperature (approximately 25°C) and positive voltage ($U = +60, +100$ kV) for different durations. Measured surface charge density of insulators is in the order of 10 μC/m^2. Range of the color scale is ± 30 μC/m^2. From the two sets of measurement results, abdominal area of the three-post insulator is positively charged with identical polarity as the DC voltage, while leg area accumulates heteropolar charges. In each set of experiments, surface charge profile pattern forms in the initial period of charge accumulation and almost does not change with increasing duration. However, charge density increases with increasing duration. After 12 hours, charge accumulation process becomes very slow and approaches equilibrium state. Therefore, it is inferred that equilibration time of charge accumulation at ambient temperature is approximately 12 hours. Moreover, comparison of Fig. 5(a) and Fig. 5(c) demonstrates that surface charge density raises with voltage amplitude, while overall charge distribution is less affected by voltage amplitude.

Temporal changes in surface charge profiles under negative voltage ($U = -60, -100$ kV) are shown in Fig. 6. The abdominal area of three-post insulator is negatively charged, and leg area is positively charged. Distribution patterns show many characteristics in polarity just opposite the situations under positive voltage. Surface charge changes with voltage amplitude and time under different polarity voltages are similar, and equilibration time of charge accumulation under negative voltage is also 12 hours.

Three-post insulators have certain rotational symmetry, and surface charge profiles of the three posts are similar. Therefore, surface curve AB of a single post from A (bottom of leg) to B (center of the abdomen) is selected as the characteristic curve to further analyze change of surface charge density for different durations. Fig. 7 presents a typical example of charge profile on characteristic curve of the three-post insulator under +100 kV. Bottom area of the leg ($l < 34$ mm) accumulates negative charges, which is contrary to polarity of the DC voltage, forming a heteropolar charge peak I. Top area of the leg and abdomen area ($l > 34$ mm) accumulate positive charges, which are the same the polarity of the DC voltage, forming two homopolar charge peaks II and III, and

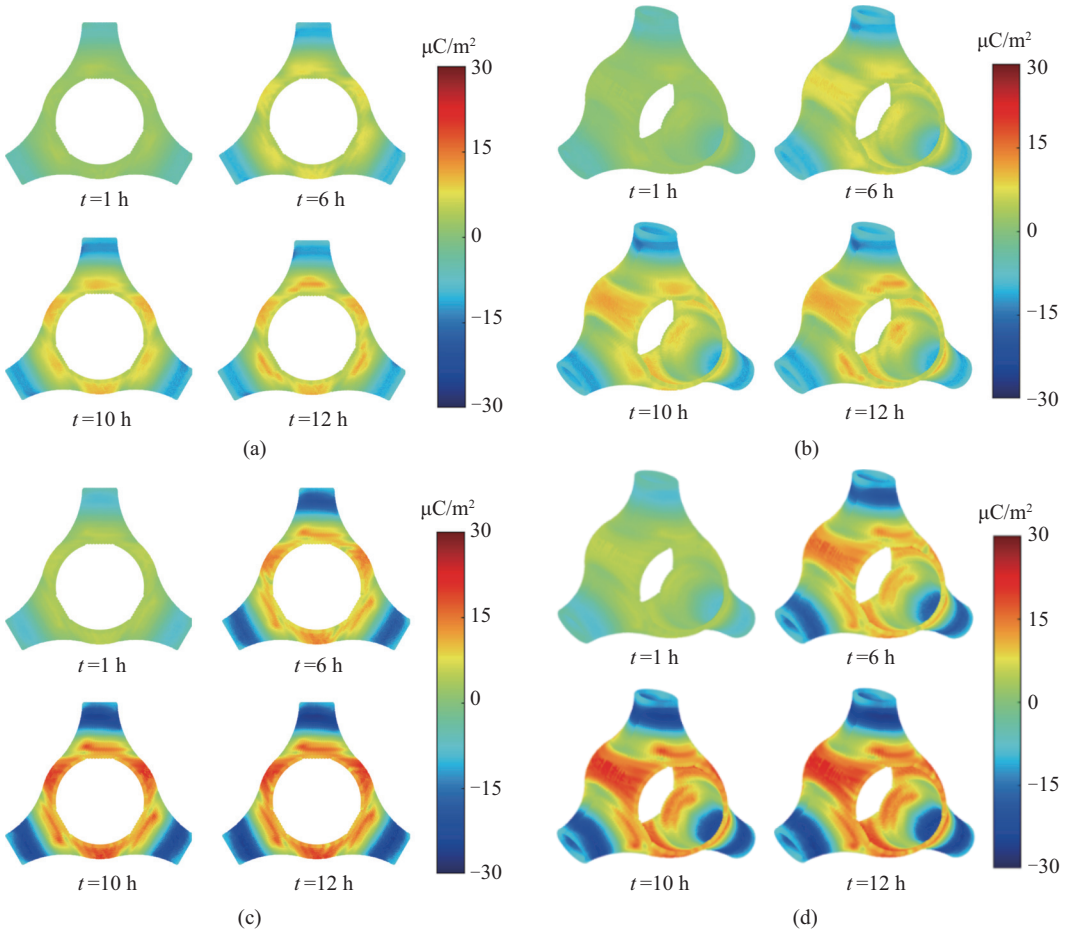

Fig. 5. Surface charge accumulation of three-post insulator under positive DC voltage. (a) Charge distribution under +60 kV. (b) 3D view of charge distribution under +60 kV. (c) Charge distribution under +100 kV. (d) 3D view of charge distribution under +100 kV.

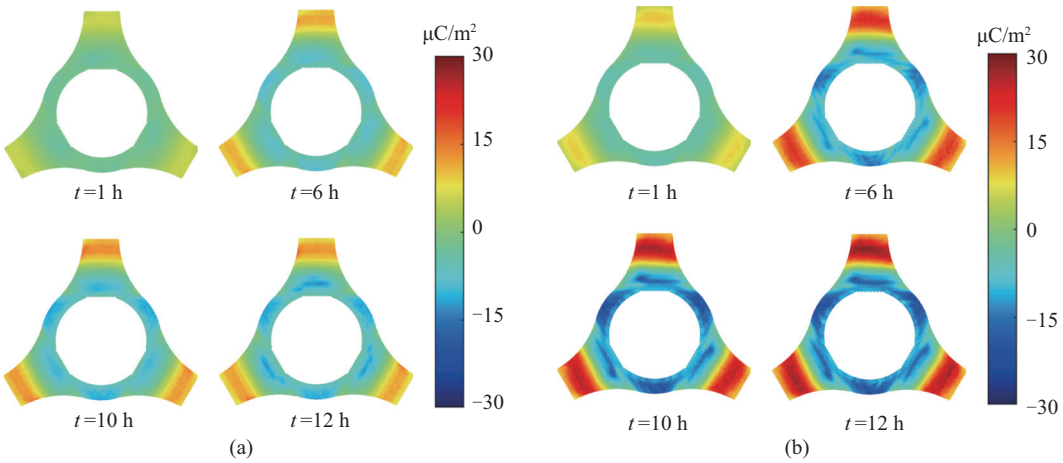

Fig. 6. Surface charge accumulation of three-post insulator under negative DC voltage. (a) −60 kV. (b) −100 kV.

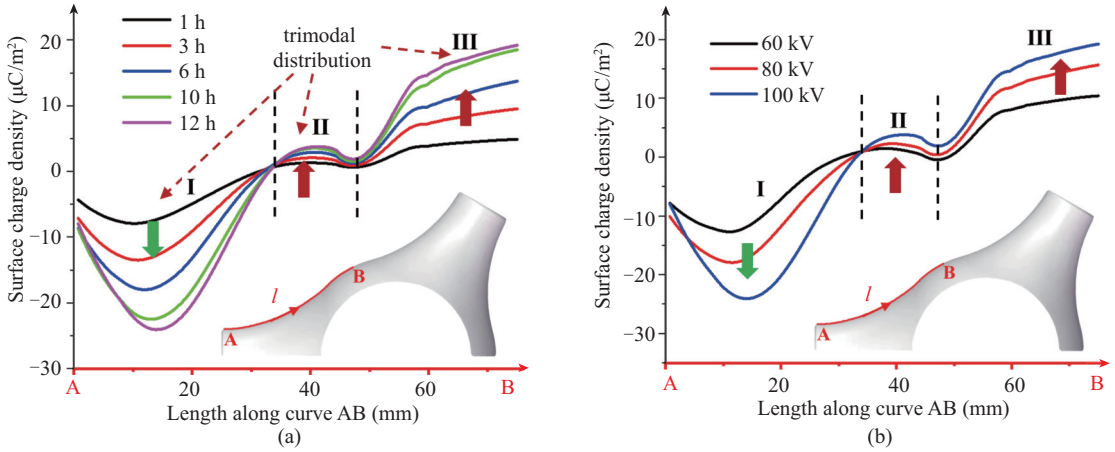

Fig. 7. Surface charge accumulation on characteristic curve of three-post insulator. (a) Change in charge density with time (+100 kV). (b) Change in charge density with voltage amplitude (12 h).

surface charge density presents a trimodal distribution. The accumulated charge density profile on the characteristic curve AB is approximately the same under different durations. In the area of each charge peak, charge density increases with increasing duration, but increased rate of diverse charge peaks is various. Fig. 7(b) exhibits change of the accumulated charge density on the characteristic curve AB with diverse voltage amplitudes. The increase of voltage amplitude to a certain extent only increases charge density but has little effect on overall charge distribution, and surface charge density still presents a trimodal distribution.

B. Effect of Temperature Gradient on Surface Charge Accumulation

During normal operating conditions, temperature range of the GIL center conductive pole is 50∼70°C, while temperature of its metal enclosure is slightly higher than ambient temperature, thus forming a temperature gradient field inside the GIL [21]. In this paper, an oil bath circulating heating device is used to heat the central conductive pole, keeping temperature at 50°C, 60°C, and 70°C, respectively. We used an infrared camera to observe temperature distribution of the three-post insulator after heating. Fig. 8 presents an example of

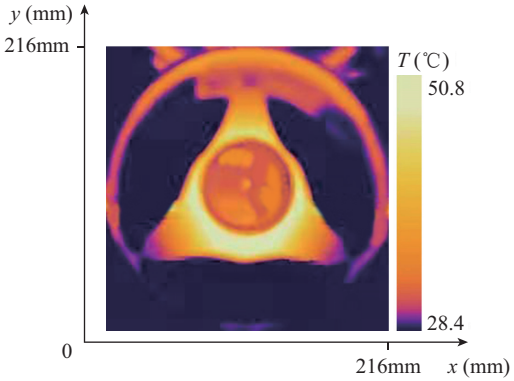

Fig. 8. Temperature distribution of three-post insulator.

temperature distribution of the three-post insulator when center conductive pole temperature $T_{\max}$ is 50°C. It can be seen that temperature of the three-post insulator shows a gradient decreasing trend from center conductive pole to enclosure. Based on established temperature gradient field, +100 kV DC voltage is put on the center conductive pole to test charge density of DC three-post insulator under influence of different temperature gradients.

Figure 9 shows surface charge profiles of the three-post insulator for different durations when temperature of the center conductive pole is 50°C and DC voltage is +100 kV. Range of the color scale is ± 60 μC/m^2. Fig. 9(a) exhibits that under the influence of the temperature gradient, only the bottom area of the leg of the three-post insulator is negatively charged, and remaining areas are positively charged. Maximum surface charge density occurs in insulator leg area. Fig. 9(c) exhibits the charge distributions on the characteristic curve AB. Surface charge density still exhibits a trimodal distribution, but amplitude and distribution range of the homopolar charge peak II in the leg region are significantly increased. The surface of the legs becomes the area where surface charge is most concentrated. Outline of the charge distribution on the characteristic curve for different durations is approximately the same. In the area of each charge peak, charge density gradually increases with increasing duration. When duration exceeds 6 hours, charge density tends to be saturated. Therefore, time interval of surface charge accumulation images selected to display is shorter, which can better reflect influence of temperature on surface charge accumulation.

Figure 10 exhibits surface charge profiles of the three-post insulator for various durations under diverse temperature gradients (+100 kV DC voltage). Range of color scale is ± 120 μC/m^2. In Fig. 10, increase of the temperature gradient will further magnify homopolar charge peak at the legs. As temperature rises, charge density of peak I at the bottom of the leg increases slightly, and charge density of peak II in the leg area increases significantly, and position of maximum charge density tends to move toward the bottom of insulator leg. Charge density of peak III in the abdomen area does not change much.

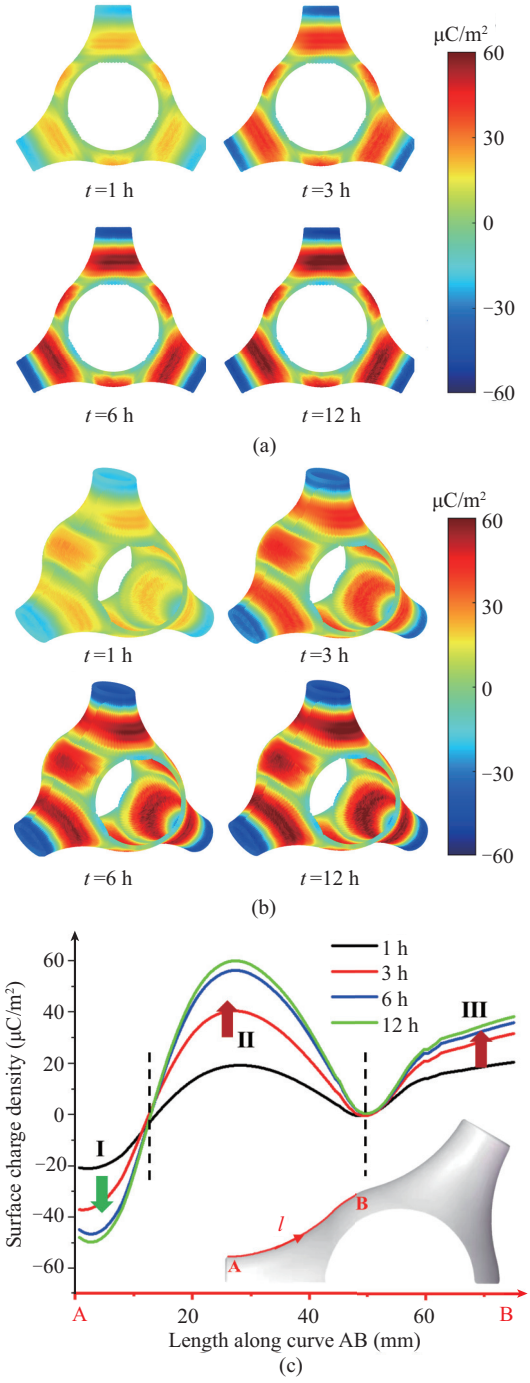

Fig. 9. Surface charge accumulation of three-post insulator under temperature gradient (+100 kV DC voltage, T_{max} = 50°C). (a) Overall charge distribution. (b) 3D view of charge distribution. (c) Charge distribution on characteristic curve.

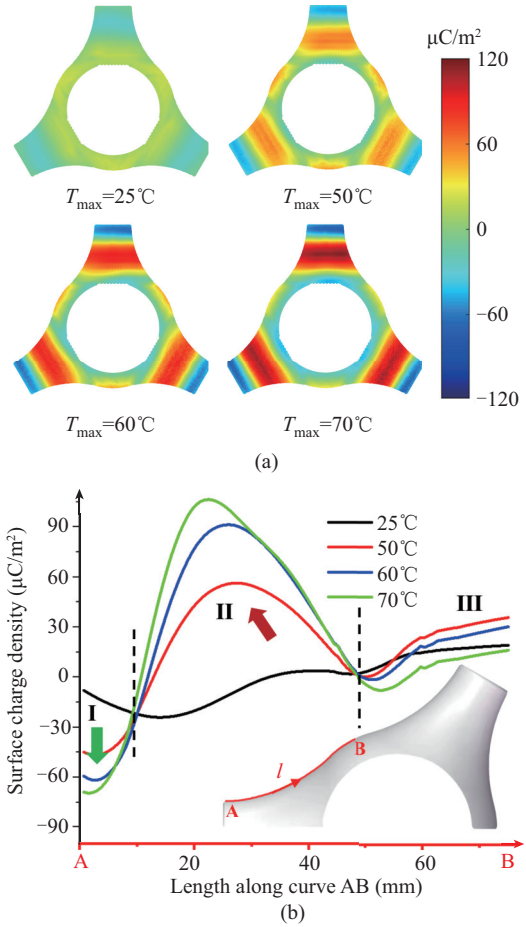

Fig. 10. Surface charge accumulation of three-post insulator under different temperatures (+100 kV DC voltage, equilibration time). (a) Overall charge distribution. (b) Charge distribution on characteristic curve.

IV. Discussion

To better understand regularity of surface charge accumulation on three-post insulators, it is essential to conduct an in-depth analysis on its mechanism. Currently, three main sources of surface charge on insulators are generally acknowledged: bulk conduction current $\boldsymbol{j}_{\mathrm{v}}$, gas conduction current $\boldsymbol{j}_{\mathrm{g}}$, and conduction current $\boldsymbol{j}_{\mathrm{s}}$ along the surface of the insulator [22]. The surface charge accumulation transient equation derived from current continuity equation can be represented as (3).

$$\frac{\partial \sigma}{\partial t} = \boldsymbol{n} \cdot \boldsymbol{j}_{\mathrm{v}} - \boldsymbol{n} \cdot \boldsymbol{j}_{\mathrm{g}} - \nabla \cdot \boldsymbol{j}_{\mathrm{s}} \tag{3}$$

where σ represents surface charge density, t is time, and $\boldsymbol{n}$ is normal vector of the insulator surface from bulk to gas.

Bulk conduction current $\boldsymbol{j}_{\mathrm{v}}$ and gas conduction current $\boldsymbol{j}_{\mathrm{g}}$ of the insulator are conducted to insulator surface along the normal direction, which is bound up with normal electric field intensity and can be expressed in (4). Furthermore, although $\boldsymbol{j}_{\mathrm{g}}$ mainly depends on positive and negative ions generated by gas ionization, gas conductivity can be adopted to simplify the description in the absence of significant partial discharges.

$$\boldsymbol{n} \cdot \boldsymbol{j}_{\mathrm{v}} - \boldsymbol{n} \cdot \boldsymbol{j}_{\mathrm{g}} = \gamma_{\mathrm{v}}(T) \cdot E_{\mathrm{Vn}} - \gamma_{\mathrm{g}}(T) \cdot E_{\mathrm{Gn}} \tag{4}$$

where γ_{v} and γ_{g} are bulk and gas material electrical conductivity, which are strongly affected by temperature T. E_{Vn} and E_{Gn} represent normal electric field intensity on bulk and gas.

Surface current $\boldsymbol{j}_{\mathrm{s}}$ makes charge flow along tangential direction, which is bound up with tangential electric field intensity and can be expressed in (5).

$$-\nabla \cdot \boldsymbol{j}_{\mathrm{s}} = -\nabla \cdot (\gamma_{\mathrm{s}}(T) \cdot \boldsymbol{E}_{\mathrm{s}}) \tag{5}$$

where γ_{s} is surface conductivity of insulation material; $\boldsymbol{E}_{\mathrm{s}}$ represents tangential electric field intensity on the surface of insulator. fon number of accumulated charges Based on the above analysis, surface charge accumulation process of insulators is mainly affected by electric field intensity and material conductivity. At ambient temperature (approximately 25°C), bulk and surface conductivity of material at various positions are equal, and gas conductivity is slightly different. The surface charge accumulation process is principally determined by surface electric field profile on the insulator.

Figure 11 is simulation result of initial capacitive electric field distribution for the three-post insulator, which is calculated by COMSOL software. In the simulation, relative permittivity of the insulator material and SF_6 gas are set to 4.95 and 1.002, respectively, and high-voltage electrode voltage is 100 kV. Surface tangential electric field intensity $\boldsymbol{E}_{\mathrm{s}}$ is mainly concentrated in the leg area (A2). Tangential field intensity in the bottom of the leg area (A1) and the abdominal area (B) is tiny and can be ignored. Surface charge accumulation in A1 and B area is mainly affected by normal current, which is bound up with normal current discrepancy of solid-gas interface. When bulk conduction current plays a dominant role, $\boldsymbol{n} \cdot \boldsymbol{j}_{\mathrm{v}} > \boldsymbol{n} \cdot \boldsymbol{j}_{\mathrm{g}}$, charge accumulated on the insulator's abdomen has identical polarity as DC voltage; when gas conduction current plays a dominant role, $\boldsymbol{n} \cdot \boldsymbol{j}_{\mathrm{v}} < \boldsymbol{n} \cdot \boldsymbol{j}_{\mathrm{g}}$, charge is contrary to polarity of the DC voltage.

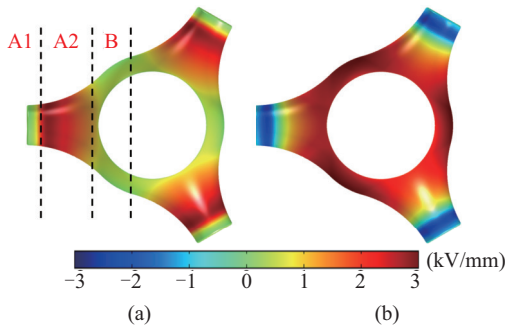

Fig. 11. Surface electric field profile of three-post insulator. (a) Tangential electric field intensity. (b) Normal electric field intensity.

Figures 5 and 6 exhibit the abdominal area of the three-post insulator accumulates positive charges under positive voltage and negative charges under negative voltage. Therefore, bulk conduction current is dominant in normal source of surface charge. Under impact of normal conduction current, bottom of the insulator leg area (A1) accumulates heteropolar charges, and abdominal area (B) accumulates homopolar charges, forming heteropolar charge peak I and homopolar charge peak III as Fig. 7.

For the leg area (A2) of three-post insulator, normal current causes the surface to be charged with identical polarity, and charge density diminishes gradually along the direction from the leg (A2) to the bottom (A1). Furthermore, surface tangential electric field intensity of the legs is inconsonant and increases gradually along the direction of the leg (A2) to the bottom (A1), which is $-\nabla \cdot (\gamma_{\mathrm{s}} \cdot \boldsymbol{E}_{\mathrm{s}}) < 0$. Therefore, surface conduction current makes the insulator leg accumulate heteropolar charge, especially in areas where tangential electric field intensity changes suddenly. Under combined influence of normal bulk conduction current and tangential surface conduction current, there are both homopolar and heteropolar charges on the leg area, which not only forms homopolar charge peak II but also expands distribution range of heteropolar charge peak I, as shown in Fig. 12.

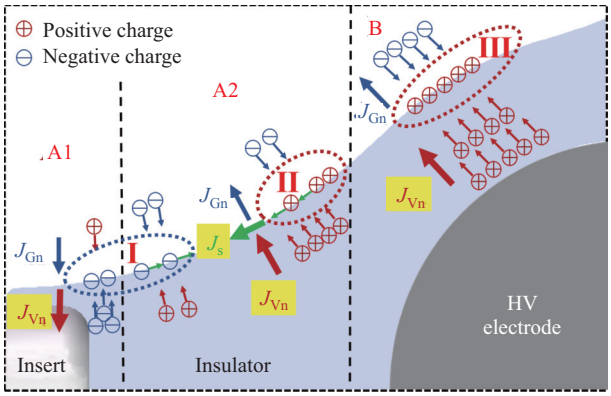

Fig. 12. Surface charge accumulation process of three-post insulator at ambient temperature.

Considering the impact of temperature gradient field, bulk and surface electrical conductivity of the insulator material rise sharply as temperature increases, thereby affecting the charge accumulation process of the three-post insulator. Surface conduction current in the bottom of the insulator leg area

(A1) and abdominal area (B) is tiny and can be ignored. Surface charge accumulation in A1 and B area is mainly affected by normal current. Figs. 9 and 10 show that the abdominal area of the insulator accumulates positive charges under positive voltage and temperature gradient, indicating that bulk conduction current is still of paramount importance in the surface charge source of A1 and B areas of the insulator under temperature gradient. However, it can be seen from Fig. 10 that surface charge density in the abdominal area does not change significantly with temperature, and increase in temperature only accelerates surface charge accumulation process and has little effect on number of accumulated charges by bulk conduction. It can be known from (4) the bulk conduction current $\boldsymbol{j}_{\mathrm{v}}$ is determined by bulk material conductivity γ_{v} and normal electric field strength E_{Vn}. Although increase in temperature leads to increase in γ_{v} and acceleration of charge accumulation, accumulated homopolar charges rapidly reduce E_{Vn} and shorten charge accumulation time of the insulator, resulting in a nearly constant total amount of charge.

For the leg area (A2) of the three-post insulator, temperature gradient not only sharply increases surface conductivity of the insulator, but also causes surface conductivity γ_{s} to decrease along the direction from leg (A2) to bottom (A1), resulting in $-\nabla\cdot(\gamma_{\mathrm{s}}\cdot\boldsymbol{E}_{\mathrm{s}})>0$. Therefore, surface conduction current causes vast homopolar charges to accumulate on the interface of the three-post insulator legs, resulting in leg area A2 becoming the region with the most concentrated charge, as presented in Fig. 13. Moreover, increase of temperature gradient results in increase of surface conductivity gradient of the material, leading to an increase in the value of $-\nabla\cdot(\gamma_{\mathrm{s}}\cdot\boldsymbol{E}_{\mathrm{s}})$. Therefore, the homopolar charge peak at the leg increases with temperature gradient.

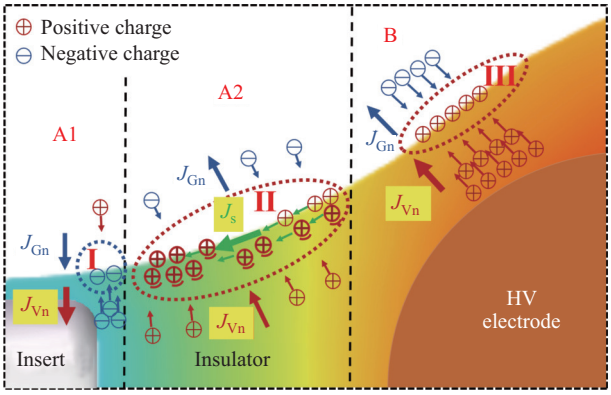

Fig. 13. Surface charge accumulation process of three-post insulator under temperature gradient.

V. Conclusion

In the present contribution, surface charge profiles of DC three-post insulators under electro-thermal coupling stress are explored by establishing a multi-degree-of-freedom movement measurement system, and dominant factors of surface charge accumulation in different areas of insulators are analyzed. Dominating conclusions are as follows:

1) At ambient temperature, the abdominal area of the three-post insulator accumulates charges of identical polarity as DC voltage, while the leg area accumulates heteropolar charges. Charge density distribution from leg bottom to center of the abdomen presents a trimodal distribution pattern, including two homopolar charge peaks and one heteropolar charge peak.

2) Under temperature gradient, only the bottom area of the legs of the three-post insulator accumulates heteropolar charges, and remaining areas accumulate homopolar charges. Amplitude and distribution range of the homopolar charge peak in the leg area increases significantly, which is the area with the most concentrated surface charge. Moreover, increase of temperature gradient will further magnify homopolar charge peak at the legs. When DC voltage is 100 kV and conductive pole temperature rises to 70°C, surface charge density of the three-post insulator can reach 100 μC/m^2.

3) Surface charge profile on the abdomen and the bottom of the legs of the DC three-post insulator is less affected by temperature, and normal bulk conduction current is of paramount importance. Surface charge accumulation process of the legs area is susceptible to temperature gradient, and inconsonant surface conductance distribution resulting from temperature gradient is the key inducement of surge in charge density. Therefore, surface conductance regulation of the leg region is the key to charge regulation and insulation optimization design of DC three-post insulators.

References

[1] T. Magier, M. Tenzer, and H. Koch, "Direct current gas-insulated transmission lines," *IEEE Transactions on Power Delivery*, vol. 33, no. 1, pp. 440–446, Feb. 2018.

[2] G. Chen, Y. P. Tu, C. Wang, J. Wang, Z. K. Yuan, G. M. Ma, J. Wang, B. Qi, and C. Y. Li, "Environment-friendly insulating gases for HVDC gas-insulated transmission lines," *CSEE Journal of Power and Energy Systems*, vol. 7, no. 3, pp. 510–529, May 2021.

[3] H. Y. Zhou, G. M. Ma, C. Wang, J. Wang, G. X. Zhang, Y. P. Tu, and C. R. Li, "Review of charge accumulation on spacers of gas insulated equipment at DC stress," *CSEE Journal of Power and Energy Systems*, vol. 6, no. 3, pp. 496–517, Sep. 2020.

[4] C. Y. Li, C. J. Lin, B. Zhang, Q. Li, W. D. Liu, J. Hu, and J. L. He, "Understanding surface charge accumulation and surface flashover on spacers in compressed gas insulation," *IEEE Transactions on Dielectrics and Electrical Insulation*, vol. 25, no. 4, pp. 1152–1166, Aug. 2018.

[5] G. M. Ma, H. Y. Zhou, Y, Wang, H. C. Zhang, S. J. Lu, Y. P. Tu, J. Wang, and C. R. Li, "Flashover behavior of cone-type spacers with inhomogeneous temperature distribution in SF_6/N_2-filled DC-GIL under lightning impulse with DC voltage superimposed," *CSEE Journal of Power and Energy Systems*, vol. 6, no. 2, pp. 427–433, Jun. 2020.

[6] S. Kumara, S. Alam, I. R. Hoque, Y. V. Serdyuk, and S. M. Gubanski, "DC flashover characteristics of a polymeric insulator in presence of surface charges," *IEEE Transactions on Dielectrics and Electrical Insulation*, vol. 19, no. 3, pp. 1084–1090, Jun. 2012.

[7] C. Y. Li, C. J. Lin, G. Chen, Y. P. Tu, Y. Zhou, Q. Li, B. Zhang, and J. L. He, "Field-dependent charging phenomenon of HVDC spacers based on dominant charge behaviors," *Applied Physics Letters*, vol. 114, no. 20, pp. 202904, May 2019.

[8] B. Y. Zhang, Z. Qi, and G. X. Zhang, "Charge accumulation patterns on spacer surface in HVDC gas-insulated system: Dominant uniform charging and random charge speckles," *IEEE Transactions on Dielectrics and Electrical Insulation*, vol. 24, no. 2, pp. 1229–1238, Apr. 2017.

[9] D. C. Faircloth and N. L. Allen, "High resolution measurements of surface charge densities on insulator surfaces," *IEEE Transactions on Dielectrics and Electrical Insulation*, vol. 10, no. 2, pp. 285–290, Apr. 2003.

[10] C. Y. Li, C. J. Lin, J. Hu, W. D. Liu, Q. Li, B. Zhang, S. He, Y. Yang, F. Liu, and J. L. He, "Novel HVDC spacers by adaptively controlling surface charges–part I: Charge transport and control strategy," *IEEE Transactions on Dielectrics and Electrical Insulation*, vol. 25, no. 4, pp. 1238–1247, Aug. 2018.

[11] J. Wang, Q. Hu, Y. N. Chang, J. R. Wang, R. X. Liang, Y. P. Tu, C. Y. Li, and Q. M. Li, "Metal particle contamination in gas-insulated switchgears/gas-insulated transmission lines," *CSEE Journal of Power and Energy Systems*, vol. 7, no. 5, pp. 1011–1025, Sep. 2021.
[12] T. Nitta and K. Nakanishi, "Charge accumulation on insulating spacers for HVDC GIS," *IEEE Transactions on Electrical Insulation*, vol. 26, no. 3, pp. 418–427, Jun. 1991.
[13] Q. Wang, G. X. Zhang, and X. X. Wang, "Characteristics and mechanisms of surface charge accumulation on a cone-type insulator under dc voltage," *IEEE Transactions on Dielectrics and Electrical Insulation*, vol. 19, no. 1, pp. 150–155, Feb. 2012.
[14] G. M. Ma, H. Y. Zhou, S. P. Liu, Y. Wang, S. J. Zhao, S. J. Lu, C. R. Li, and Y. P. Tu, "Measurement and simulation of charge accumulation on a disc spacer with electro-thermal stress in SF_6 gas," *IEEE Transactions on Dielectrics and Electrical Insulation*, vol. 25, no. 4, pp. 1221–1229, Aug. 2018.
[15] G. M. Ma, H. Y. Zhou, S. J. Lu, Y. Wang, S. P. Liu, C. R. Li, and Y. P. Tu, "Effect of material volume conductivity on surface charges accumulation on spacers under dc electro-thermal coupling stress," *IEEE Transactions on Dielectrics and Electrical Insulation*, vol. 25, no. 4, pp. 1211–1220, Aug. 2018.
[16] W. G. Li, H. Han, C. J. Gao, B. Qi, M. Huang, C. H. Zhang, X. Yang, Z. K. Huang, and J. W. Chu, "Development of a surface charge measurement system for GIL Tri-post insulator in SF_6," in *Proceedings of the IEEE 2nd International Conference on Automation, Electronics and Electrical Engineering (AUTEEE)*, Shenyang, China, 2019, pp. 35–39.
[17] B. X. Du, J. N. Dong, J. Li, H. C. Liang, and X. X. Kong, "Gas convection affecting surface charge and electric field distribution around Tri-post insulators in ±800 kV GIL," *IEEE Transactions on Dielectrics and Electrical Insulation*, vol. 28, no. 4, pp. 1372–1379, Aug. 2021.
[18] L. Zhang, C. J. Lin, C. Y. Li, S. V. Suraci, G. Chen, U. Riechert, T. Shahsavarian, M. Hikita, Y. P. Tu, Z. S. Zhang, D. Fabiani, and J. L. He, "Gas–solid interface charge characterisation techniques for HVDC GIS/GIL insulators," *High Voltage*, vol. 5, no. 2, pp. 95–109, Apr. 2020.
[19] B. Y. Zhang, W. Q. Gao, Z. Qi, Q. Wang, and G. X. Zhang, "Inversion algorithm to calculate charge density on solid dielectric surface based on surface potential measurement," *IEEE Transactions on Instrumentation and Measurement*, vol. 66, no. 12, pp. 3316–3326, Dec. 2017.
[20] S. Okabe and A. Kumada, "Measurement methods of accumulated electric charges on spacer in gas insulated switchgear," *IEEE Transactions on Power Delivery*, vol. 22, no. 3, pp. 1547–1556, Jul. 2007.
[21] B. Y. Zhang, Z. Qi, and G. X. Zhang, "Thermal gradient effects on surface charge of HVDC spacer in gas insulated system," in *Proceedings of 2016 IEEE Conference on Electrical Insulation and Dielectric Phenomena (CEIDP)*, Toronto, ON, Canada, 2016, pp. 703–706.
[22] A. Winter and J. Kindersberger, "Transient field distribution in gas-solid insulation systems under DC voltages," *IEEE Transactions on Dielectrics and Electrical Insulation*, vol. 21, no. 1, pp. 116–128, Feb. 2014.

Qi Hu received a Ph.D. degree in Electrical Engineering from North China Electric Power University, China, in 2022. He is currently an assistant engineer at State Grid Jiangxi Electric Power Co., Ltd., Nanchang, China. His current research interests include surface charge characteristics and insulation medium materials for high-voltage direct-current spacers in GIL.

Qingmin Li (M'07) received the B.S., M.S., and Ph.D. degrees in Electrical Engineering from Tsinghua University, Beijing, China, in 1991, 1994, and 1999, respectively. He is currently a professor at the North China Electric Power University, Beijing, China. His currently research interests include lightning protection of clean energy equipment, GIS/GIL insulation optimization, condition monitoring and fault diagnostics.

Zhipeng Liu received a B.S. degree with a major in Metallurgical Engineering from Taiyuan University of Technology. He is pursuing a master degree major in electrical engineering in North China Electric Power University, China. He focuses on failure of insulators for high-voltage direct-current spacers in GIL.

Naifan Xue is pursuing a Ph.D. degree at North China Electric Power University, China. His research interests include the condition monitoring, the detection of dust, and location of PD sources in high-voltage equipment.

Jian Wang received the Ph.D. degree in North China Electric Power University, Beijing, China, in 2017. He is currently an associate Professor at the North China Electric Power University, China. He mainly engages in research work on GIL insulation optimization and mechanical load carrying capacity.

Manu A. Haddad received the first degree in Electrical Engineering in 1985 and then a Ph.D. degree in High Voltage Engineering in 1990. He is now a professor at Cardiff University. His research interests are in overvoltage protection, insulation systems, insulation coordination and earthing systems. He is a member of CIGRE working groups and a member of BSI PEL1/2, IEC TC37. Prof. Haddad is a Fellow of the IET and a Fellow of the Learned Society of Wales.